

## Screening effects on the quadrupole splitting in amorphous Fe-Zr alloys

P. M. L. O. Scholte\*

*Solid State Physics Laboratory, University of Groningen, Materials Science Centre, 1 Melkweg, NL-9718 EP Groningen, The Netherlands*

M. Tegze†

*Central Research Institute for Physics, Hungarian Academy of Sciences, P.O. Box 49, H-1525 Budapest, Hungary*

F. van der Woude

*Solid State Physics Laboratory, University of Groningen, Materials Science Centre, 1 Melkweg, NL-9718 EP Groningen, The Netherlands*

(Received 6 June 1988)

The screening by the conduction electrons changes the local symmetry of the charge distribution as experienced by a local  $^{57}\text{Fe}$  probe nucleus. As a consequence the quadrupole splitting in an amorphous alloy cannot be used as a characteristic feature of the structure for identification. The concentration dependence of the quadrupole splitting in amorphous Fe-Zr alloys can be understood by assuming a transition in the electronic structure, without the assumption of a structural transition. Further evidence for such a transition has been found in the literature.

### I. INTRODUCTION

For the study of the local structure of amorphous alloys a number of techniques are available. A very successful microscopic technique is Mössbauer effect spectroscopy. Nowadays most of the local atomic structure data has been obtained using this experimental technique. In a previous paper we have shown how information can be obtained from the isomer shift about the packing and chemical interactions in amorphous alloys.<sup>1</sup> In this paper we will concentrate ourselves on the quadrupole splitting.

A commonly used method to determine the local structure from the Mössbauer spectrum is by comparing the (average) values of the hyperfine parameters and their distributions with their respective values in crystalline alloys. It should be noted that this procedure is far from unambiguous. Depending on the specific parameter that an author wants to stress, he may conclude to a different local structure. A clear example of this ambiguity is the discussion in the literature about the local structure of amorphous  $\text{FeZr}_3$ .<sup>2</sup>

However, the determination of the local structure from the Mössbauer quadrupole splitting is not a trivial task. The quadrupole splitting is directly related to the electric field gradient (EFG). This field gradient is determined by the asymmetry in the atomic and electronic structure. These two contributions cannot be separated easily. But it is obvious that they must be correlated since the atomic structure is determined by the electronic structure and vice versa. In a metal the problem generally is approached by splitting the total EFG in an ionic and an electronic term

$$V_{zz} = (1 - \gamma_\infty) V_{zz}^{\text{latt}} + V_{zz}^{\text{el}}. \quad (1)$$

$V_{zz}^{\text{latt}}$  represents the contribution from the ionic charges on the lattice sites. This contribution is amplified by the Sternheimer antishielding factor  $\gamma_\infty$ .  $V_{zz}^{\text{el}}$  is the contribu-

tion from the conduction electrons to the EFG. Generally the ionic term in (1) can be calculated in a straightforward way using lattice-sum techniques.<sup>3</sup> However, the electronic EFG is less accessible to calculations.

In 1975 Raghavan *et al.* proposed a so-called "universal" correlation between the electronic and ionic EFG.<sup>4</sup> Generally this correlation has been used to justify the interpretation of changes in the quadrupole splitting in amorphous alloys in terms of structural fluctuations, neglecting variations in the electronic structure. Recently Vianden compiled the EFG data of the pure and binary metallic systems for which presently the sign of the EFG has been determined.<sup>5</sup> He concluded that the universal correlation is destroyed. It gives an oversimplification of the contribution of the electrons to the EFG. Therefore it is necessary to take into account the electronic contribution to the EFG in a more detailed way. In this paper we propose a method to do this for amorphous alloys. The model is described in Sec. II and the effect of this contribution on the quadrupole splitting of clusters with and without chemical order is discussed. In Sec. III we will discuss the experimental quadrupole splitting in amorphous Fe-Zr alloys. Verma *et al.* showed that in crystalline Fe-Zr alloys the Rahavan coefficient is approximately 9.<sup>6</sup> This shows that the EFG in these alloys is dominated by the electronic contribution. Therefore we believe that the Fe-Zr alloys are a good system to study the effect of the electronic contribution on the quadrupole splitting. Finally, in Sec. IV we will show how the changes in the quadrupole splitting can be related to variations in the electronic structure.

### II. THEORY

In principle there are two approaches to calculate the EFG at a nucleus in a metal. The first one is to take the point-charge interaction of the ions at the lattice sites and

add to this the interaction with the conduction electrons which are described by their wave functions. The second approach is to consider the conduction electrons as a collective medium. Using pseudopotentials for the interaction between the ions and dielectric-response theory it is possible to obtain expressions for the electronic and total EFG at the nucleus. Both these methods have been reviewed by Kaufmann and Vianden<sup>7</sup> and Witthuhn and Engel.<sup>8</sup> Clearly the wave-function approach is not applicable as far as the case of amorphous alloys is concerned, since the wave functions in these alloys are not known. Therefore we will use pseudopotential theory to calculate the EFG.

### A. EFG model

We start with an <sup>57</sup>Fe probe at the origin and an ion with charge  $q$  at distance  $\mathbf{r}$  embedded in an electron gas. The total potential experienced by the probe atom can be written as

$$\Phi(\mathbf{r}) = \Phi_C(\mathbf{r}) + \Phi_{sc}(\mathbf{r}). \quad (2)$$

$\Phi_C(\mathbf{r})$  denotes the bare (Coulomb) potential of the ion and  $\Phi_{sc}(\mathbf{r})$  is the potential due to the screening electrons. Using dielectric-response theory we can write for the total screened potential

$$\Phi(\mathbf{r}) = \frac{1}{4\pi\epsilon_0} s(r, \lambda) \frac{q}{r}. \quad (3)$$

$s(r, \lambda)$  contains the screening term which depends on the screening length  $\lambda$ . Then the electric field gradient can be written as

$$v_{ij} = \frac{q}{4\pi\epsilon_0} S(r, \lambda) \frac{3x_i x_j - r^2 \delta_{ij}}{r^5} \quad (4)$$

and the screening of the electrons is represented by the term  $S(r, \lambda)$ .

The screening of a charge by a free-electron gas cannot be calculated exactly from the free-electron dielectric function. In the case that the screened potential is a slowly varying function of  $r$  with respect to the interatomic spacing we only have to consider the first few terms of the Fourier expansion of the dielectric function. This leads to the so-called Thomas-Fermi screening. A different approximation of the screening is obtained by making an asymptotic expansion of the dielectric function around its logarithmic singularity at  $k = 2k_f$ , where  $k_f$  is the Fermi wave vector. This approximation is known as the Lindhard approximation. It must be stressed that Thomas-Fermi screening cannot be considered as a limiting case of Lindhard screening. In fact, they are approximations of the dielectric function at different points.

In the simple case of Thomas-Fermi (TF) screening one finds, with  $\rho = r/\lambda$ ,

$$S_{TF}(r, \lambda_{TF}) = (1 + \rho + \frac{1}{3}\rho^2) e^{-\rho}, \quad (5a)$$

$$\frac{1}{\lambda_{TF}^2} = \frac{e^2}{\epsilon_0} \frac{n(E_f)}{V_m}, \quad (5b)$$

where  $n(E_f)$  is the (free-electron) density of states at the Fermi level and  $V_m$  is the molar volume. For Lindhard screening we have<sup>7</sup>

$$S_L(r, \lambda) = A \left[ \begin{aligned} & [3 - \rho^2 + 3B(\ln\rho + \gamma')] \frac{\cos\rho}{\rho^2} \\ & + [3\rho^2 + B(\rho^2 - 3)(\ln\rho + \gamma')] \frac{\sin\rho}{\rho^3} \end{aligned} \right], \quad (6a)$$

with

$$A = \frac{2\pi}{3} \frac{a_0/\lambda_L}{(1 + \pi a_0/\lambda_L)^2}, \quad (6b)$$

$$B = \frac{4}{1 + \pi a_0/\lambda_L}, \quad (6c)$$

$$\gamma' = \gamma + \ln 2 - \frac{3}{2}, \quad (6d)$$

$$\frac{1}{\lambda_L} = 2k_f, \quad (6e)$$

where  $\gamma = 0.5772156649\dots$  is Euler's constant.  $a_0$  is the Bohr radius and the Fermi wave number  $k_f$  is defined in terms of the effective number of free electrons per atom  $Z^*$  (Ref. 9),

$$k_f^3 = 3\pi^2 \frac{N_A Z^*}{V_m}, \quad (6f)$$

where  $N_A$  is Avogadro's number.

When we have only free electrons the Lindhard screening length can be related to the Thomas-Fermi screening length

$$\lambda_L = \frac{2\lambda_{TF}^2}{\pi a_0} \quad (7)$$

Now the total EFG experienced by the nucleus at the origin due to the surrounding ions is

$$v_{ij}^{at}(\mathbf{0}) = \alpha(1 - \gamma_\infty) \sum_n^{\text{ions}} v_{ij}(r_n). \quad (8)$$

We have written the antishielding factor as  $\alpha(1 - \gamma_\infty)$ .  $\gamma_\infty$  is the Sternheimer antishielding factor for the free ion. In a metal the charge distribution around the nucleus is almost neutral because of the strong screening. The antishielding factor should be appropriate to this almost neutral charge distribution, and so is expected to be larger than the free-ion value.<sup>10</sup> This antishielding enhancement is represented by the factor  $\alpha$ .

The summation in (8) is calculated over the nearest neighbors of the central Fe atom. In crystalline materials with long-range order (LRO) this may lead to erroneous results, but because of the absence of LRO in amorphous alloys the symmetry of the next coordination shells becomes more spherical. As a consequence the contribution of these shells will be small. Also the introduction of the screening term causes the lattice sum to converge more rapidly. We also calculated the absolute value of the quadrupole splitting only; this parameter can be obtained readily from Mössbauer experiments, while the

sign of the quadrupole splitting must be determined using external magnetic fields.

### B. Atomic model

We have used two different types of clusters to represent amorphous structures. The first class of clusters has been constructed using the algorithm of Finney and Bennett<sup>11</sup> to construct a dense random packing of hard spheres (DRPHS). The resulting clusters consisted out of 1500 spheres with two different radii. The packing fraction of the clusters was 0.65. Experimental values of the packing fraction in a number of transition-metal-metalloid alloys are in the range 0.65–0.74.<sup>12</sup> The packing fractions of our DRPHS clusters are at the lower boundary of this range. Expanding the cluster will lower the packing fraction further.

The second category clusters have been constructed by surrounding a central Fe atom with a crystalline cell. The sites of this cell are randomly occupied by two different point atoms. Next the radial distances are 5% randomly distorted. This value is a reasonable estimate of the broadening of the radial distribution function due to the structural disorder.<sup>13</sup> These clusters still have some reminiscences of the original crystalline units by the angular correlations which are conserved.

To characterize the atoms we have used the well-known Miedema parameters. In Table I we have listed the relevant parameters for some elements. The ionic charge is calculated assuming that

$$q_0(\cdot)N_{ws}V_m, \quad (9)$$

where  $V_m$  is the molar volume and  $N_{ws}$  the Miedema electronic density at the Wigner-Seitz cell boundary. When the atoms are put together in an alloy the atomic charge and their size change due to charge transfer. We have corrected them using the model of Miedema and Niessen.<sup>14,15</sup> The atomic radii are calculated from the partial molar volumes using a packing fraction of 0.65. In the pseudocrystalline models the nearest-neighbor distance is the sum of these radii.

### C. Computer simulations

For the moment we will neglect the screening term in (4), i.e., we set  $S(r, \lambda) = 1$ . In general we can distinguish two sources for the EFG. The first source is the lattice distortion and the second one is the chemical disorder. We will define two “standard” clusters to study these.

TABLE I. (Bulk) Parameters of the pure elements.  $\Phi^*$  and  $N_{ws}$  are the Miedema parameters [1 d.u. (density unit) is approximately  $4.7 \times 10^{22} e/cm^3$ ],  $V_m$  is the molar volume, and  $q_0$  is the ionic charge calculated from  $N_{ws}$ .

Element	$\Phi^*$ (V)	$N_{ws}$ (d.u.)	$V_m$ (cm <sup>3</sup> )	$q_0$ (e)
Fe	4.93	5.55	7.10	3
Zr	3.40	2.69	14.10	3
Hf	3.55	2.92	13.60	3
B	4.75	3.72	4.60	1.3

Both are constructed from the nearest-neighbor shell of a fcc lattice with the nearest-neighbor distance 1 Å; i.e., they consist out of 12 atoms, our central probe atom not included. Standard cluster 1 is left undistorted and on the sites we put randomly atoms  $A$  and  $B$  with charge  $+e$  and  $-e$  respectively. The radial distances in standard cluster 2 are 5% distorted randomly and the sites are occupied by atoms with charge  $e$ .

The contribution from the lattice distortion can be calculated from standard cluster 2 and amounts  $|\overline{\Delta E_Q^{latt}}| = 3.09$  mm/sec. In a binary alloy this contribution is proportional to the average ionic charge. The lattice contribution is independent of the composition, when the average ionic charge is constant.

The chemical contribution is proportional to the charge difference of the ions in the cluster. It has a maximum at the equiatomic composition of  $|\Delta E_Q^{chem}| = 10.17$  mm/sec. This maximum merely reflects the maximum in the probability to generate asymmetric clusters at this composition.

In Fig. 1 we show the chemical and lattice contribution to the quadrupole splitting in a distorted fcc-like cluster. It must be noted that both contributions are of the same order of magnitude. These contributions are not simply additive, since the EFG due to the chemical disorder generally will not be along the same direction as the EFG due to the lattice distortion. We can make a crude approximation to the total quadrupole splitting in a fcc-like cluster with nearest-neighbor (NN) distance  $R_{NN}$ :

$$\Delta E_Q^{tot}(x, \delta) \approx \frac{\{[\langle q \rangle |\overline{\Delta E_Q^{latt}}(\delta)|]^2 + [\Delta q |\overline{\Delta E_Q^{chem}}(x)|]^2\}^{1/2}}{R_{NN}^3}, \quad (10)$$

with

$$\langle q \rangle = q_A x / 100 + q_B (1 - x / 100), \quad (11a)$$

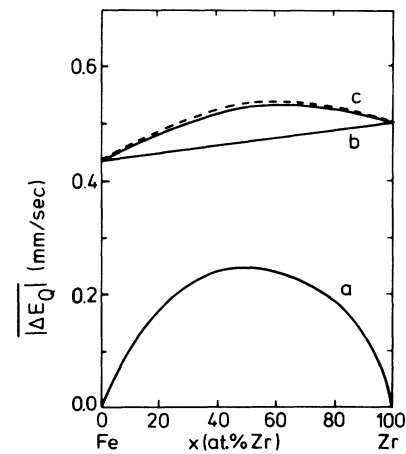


FIG. 1. Quadrupole splitting in a distorted fcc cluster of nearest neighbors with nearest-neighbor distance  $R_{NN} = 2.74$  Å,  $q_A = 3e$ ,  $q_B = 3.5e$ , and distortion  $\delta = 0.05$ . One should note that the chemical contribution increases due to the increase of the average charge only. (a) Chemical contribution, (b) contribution due to the lattice distortion, and (c) total quadrupole splitting (solid line); the dashed line is explained in the text.

$$\Delta q = q_A - q_B \quad (11b)$$

$q_A$  and  $q_B$  are the ionic charges of atom  $A$  and  $B$ , respectively and  $x$  is the concentration of atom  $A$ .  $|\Delta E_Q^{\text{latt}}(\delta)|$  and  $|\Delta E_Q^{\text{chem}}(x)|$  are calculated using the previously described standard clusters;  $\delta$  gives the distortion of the radial distances ( $\delta=0.05$  in standard cluster 2). In fact, (10) states only that we have two uncorrelated contributions to the total quadrupole splitting: one from the lattice distortion, which is proportional to the average ionic charge, and a second from the chemical disorder, proportional to the charge difference only. In general these contributions will be correlated, since the lattice distortion will influence the chemical term, too. In Fig. 1(c) the total quadrupole splitting in a fcc-like cluster of 12 atoms is shown. The dashed curve has been calculated using Eq. (10). It is seen that this curve is a reasonable description of the simulated points. This means that the correlation between the chemical and the lattice term is small.

Now consider the influence of screening on the quadrupole splitting. We have calculated the quadrupole splitting in a distorted fcc cluster of Fe- and Zr-like atoms, using Lindhard screening and Thomas-Fermi screening with  $Z^*=1, 2,$  and  $3$ . The respective screening lengths have been calculated from (6f) and (7). The molar volume and the ionic charges were corrected for charge transfer. The results are shown in Figs. 2 and 3. In the Thomas-Fermi case the qualitative behavior of the composition dependence of the quadrupole splitting flattens with increasing screening, but it does not change dramatically. In the Lindhard case the characteristics of the composition dependence change completely, depending on the effective number of free electrons per atom. The quadrupole splitting is dominated by the contribution of the conduction electrons. The ionic charges are screened effectively and become almost "neutral." As a result the quadrupole splitting is not dominated anymore by the chemical disorder but by the lattice distortion or, more precisely, by the variation of the nearest-neighbor distance with composition.

Finally, we will consider the effect of screening on the

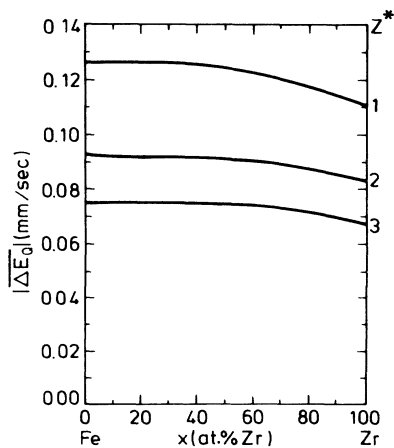


FIG. 2. Quadrupole splitting in an amorphous fcc nearest-neighbor cluster with Thomas-Fermi screening for different values of the effective number of free electrons  $Z^*$ .

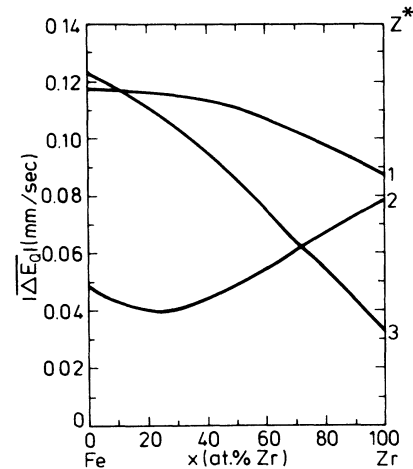


FIG. 3. Quadrupole splitting in an amorphous fcc nearest-neighbor cluster with Lindhard screening for different values of  $Z^*$ .

quadrupole splitting and asymmetry parameter of a number of clusters with chemical order. As an example we will take  $\text{Fe}_3\text{B}$ . Tegze *et al.* have calculated the density of states for this alloy in different structures. They concluded that the electronic structure is not sensitive to minor changes in the atomic positions, but that it depends strongly on the local order.<sup>16</sup> The structures they used were, respectively, the body-centered  $\text{Ni}_3\text{P}$  structure, the orthorhombic  $\text{Ni}_3\text{B}$  structure, the bcc-like  $\text{Fe}_3\text{Al}$ , and the fcc-like  $\text{Cu}_3\text{Au}$  structure.

We have calculated the quadrupole splitting in the nearest-neighbor clusters surrounding the Fe sites in these structures. The original chemical short-range order was conserved, i.e., the sites in the cluster were not occupied in a random way. For the ionic charges of the Fe and B atoms the values of Table I have been used. The charge transfer between Fe and B was found to be negligible. To account for the electronic contribution to the EFG we have used Lindhard screening, with antishielding enhancement factor  $\alpha=6.1$ . This is a representative value for the antishielding enhancement as we will see in the next paragraph. We have taken the value  $Z^*=2$  for the effective number of free electrons per atom, in accordance with the values for  $\text{Co}_{81}\text{P}_{19}$  and  $\text{Ni}_{81}\text{P}_{19}$  proposed by Eposito *et al.*<sup>9</sup> This gives for the screening length  $\lambda_L=0.277 \text{ \AA}$ .

The results of the calculations are shown in Table II. The effect of the conduction electrons is not a simple amplification factor of the ionic contribution, as is assumed by the universal correlation. Both the sign and magnitude of the quadrupole splitting are affected, as well as the asymmetry parameter  $\eta$ . From these results we conclude that the charge asymmetry as experienced by the central probe atom is changed by the screening charge of the conduction electrons. When we compare the results for the different clusters we see that the change depends strongly on the local order around the probe atom. It can be concluded that a comparison between the sign and magnitude of the quadrupole splitting

TABLE II. Quadrupole splitting  $\Delta E_Q$  and asymmetry parameter  $\eta$  in a number of nearest-neighbor clusters with chemical order, without screening and with Lindhard screening with screening length  $\lambda_L = 0.277 \text{ \AA}$ . All  $\Delta E_Q$  are in mm/sec. (o indicates orthorhombic and bct indicates body-centered tetragonal).

Structure site	bct (Ni <sub>3</sub> P)						o (Ni <sub>3</sub> B)				bcc		fcc	
	1		2		3		1		2		1	2	1	
	$\Delta E_Q$	$\eta$	$\Delta E_Q$	$\eta$	$\Delta E_Q$	$\eta$	$\Delta E_Q$	$\eta$	$\Delta E_Q$	$\eta$	$\Delta E_Q$	$\Delta E_Q$	$\Delta E_Q$	$\eta$
No screening	-0.52	0.09	+0.88	0.80	-0.45	0.92	-0.81	0.78	-0.66	0.44	0	0	+1.45	0
Lindhard	-0.31	0.85	+0.58	0.75	+0.40	0.64	+0.38	0.94	-0.66	0.32	0	0	+0.73	0

and asymmetry parameter in crystalline and amorphous alloys is meaningless when the differences in the electronic structure are not considered as well.

### III. AMORPHOUS Fe-Zr ALLOYS

Now let us consider the quadrupole splitting in amorphous Fe-Zr alloys. Amorphous ribbons of approximately 1 mm wide and 20  $\mu\text{m}$  thick have been prepared by means of melt spinning in an atmosphere of purified argon. This amorphous layers of about 5000  $\text{\AA}$  were produced by two source coevaporation of Fe and Zr onto an quartz or aluminum substrate in UHV equipment.<sup>17</sup> The noncrystallinity of these samples was confirmed by x-ray diffraction.

The quadrupole splitting in these alloys was determined by measuring the room-temperature Mössbauer spectra. The spectra were recorded using a conventional constant-acceleration-type spectrometer with a moving source (<sup>57</sup>Co in Rh) and a stationary absorber. To eliminate substrate effects and to reduce the measuring time we used conversion-electron Mössbauer spectroscopy (CEMS) to obtain the spectra of the thin films. Some films were measured also in transmission geometry, but the spectra were identical to the CEMS spectra. To analyze the spectra the Fourier-deconvolution method of Vincze<sup>15,18</sup> was used.

In Fig. 4 the Mössbauer spectra and resulting distribution functions are shown. In Fig. 5 we show the average absolute quadrupole splitting deduced from these distribution functions. The isomer shift has been discussed in a previous paper.<sup>1</sup> It can be seen from Fig. 5 that there is no systematic difference between the quadrupole splitting of alloys produced by melt quenching and by coevaporation. Therefore we will make no distinction between these samples. In Fig. 5 we have included also the quadrupole splitting in a number of amorphous Fe-Hf alloys. This system follows the same trend as the Fe-Zr alloys. This is not surprising since Zr and Hf are very similar as far as their atomic parameters are concerned (see Table I).

Let us first neglect the screening by the conduction electrons. In Fig. 6 we show the quadrupole splitting in a number of nearest-neighbor clusters. It can be seen that the quadrupole splitting scales with the number of nearest neighbors. The qualitative behavior is in all cases the same. One should note also the correspondence in the quadrupole splitting of the DRPHS clusters, which is not a point-charge model and the pseudocrystalline fcc-like cluster of point charges. Due to the chemical disorder the composition dependence is a smooth convex func-

tion. The slow decrease of the quadrupole splitting is due to the increase of the nearest-neighbor distance and the decrease of the charge difference with increasing Zr content. It is clear that we cannot explain the experimental quadrupole splitting when we neglect the screening, without assuming a structural transition.

However, we have seen in Sec. II that the introduction of Lindhard screening completely changes the concentration dependence of the simulated quadrupole splitting. To simulate the quadrupole splitting in amorphous Fe-Zr alloys we used a distorted fcc-like nearest-neighbor cluster around a central Fe atom. To obtain an average the quadrupole splitting was calculated over 1000 different clusters.

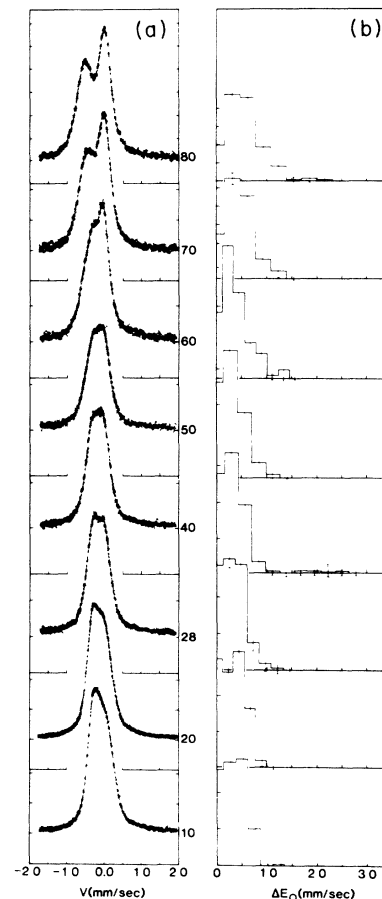


FIG. 4. Room-temperature Mössbauer spectra and quadrupole splitting distribution functions of amorphous Fe<sub>100-x</sub>Zr<sub>x</sub> alloys.

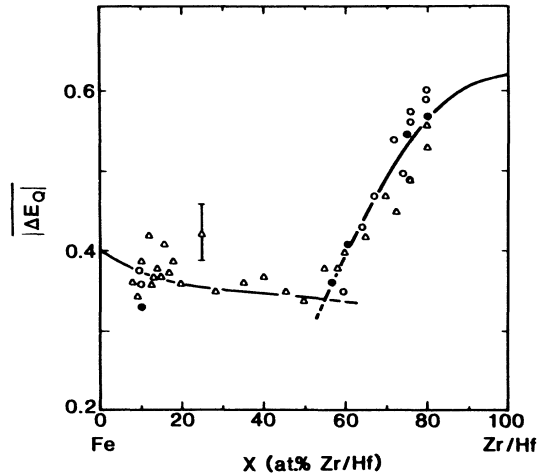


FIG. 5. Average quadrupole splitting of amorphous  $\text{Fe}_{100-x}\text{Zr}_x$  ( $\circ, \triangle$ ) and  $\text{Fe}_{100-x}\text{Hf}_x$  ( $\bullet$ ) alloys. Alloys indicated with ( $\circ, \bullet$ ) have been prepared by melt quenching; alloys indicated by ( $\triangle$ ) have been produced by coevaporation.

The problem we are immediately confronted with is to make a reliable estimate for the effective number of free electrons per atom  $Z^*$ . We cannot deduce  $Z^*$  directly from the experimental quadrupole splitting, since we also have to determine the antishielding enhancement factor  $\alpha$ . However, some information about  $Z^*$  can be deduced from resistivity measurements. Buschow *et al.* have investigated the temperature coefficient of the resistivity (TCR) in amorphous (Fe, Co, Ni)-Zr alloys.<sup>19</sup> They found that all these alloys had a negative TCR in the high-temperature limit. The diffraction model for liquid alloys predicts a negative TCR when  $Q_p = 2k_f$ , where  $Q_p$  is the principal maximum in the x-ray interference function. In amorphous alloys this peak is rather broad, so Buschow *et al.* proposed a somewhat relaxed condition for a negative TCR (Ref. 19)

$$2k_f = Q_p \pm 0.2 \text{ \AA}^{-1}. \quad (12)$$

A simple choice for  $Z^*$  that reproduces the behavior of

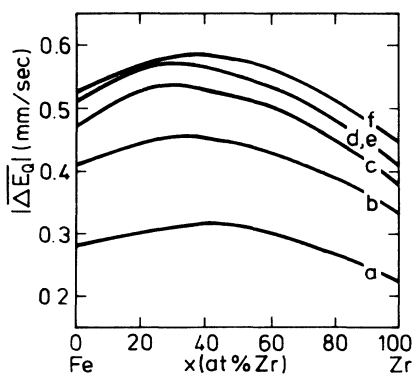


FIG. 6. Average quadrupole splitting in simulated amorphous nearest-neighbor clusters without screening: (a) tetrahedron, (b) bcc with 8 neighbors, (c) bcc with 14 neighbors, (d) fcc, (e) dodecahedron, and (f) DRPHS cluster.

the experimental quadrupole splitting, and that is in accordance with this condition is

$$Z^* = \begin{cases} 1.44x_{\text{Fe}} + 2.36x_{\text{Zr}}, & x_{\text{Zr}} < 55 \\ 2.66x_{\text{Fe}} + 1.36x_{\text{Zr}}, & x_{\text{Zr}} > 55. \end{cases} \quad (13)$$

$x_{\text{Fe}}$  and  $x_{\text{Zr}}$  are the atomic concentrations of Fe and Zr, respectively.

In Fig. 7 we have plotted  $Z^*$  and the resulting values for  $2k_f$ . It can be seen that the values of  $2k_f$  lie within the range defined by (12). One should be aware that the values of  $Z^*$  and  $\alpha$  are heavily correlated. Within the experimental accuracy the quadrupole splitting can be reproduced using different values for  $Z^*$  and  $\alpha$ . However, then it is not possible to fulfill (12) over the whole concentration range. In Fig. 5 we have plotted the resulting quadrupole splitting, using  $\alpha = 6.1$ . The fit to the experimental points is satisfying. Furthermore, the value of  $\alpha$  is in good agreement with the values used by Sholl<sup>10</sup> and Nishiyama.<sup>20</sup>

#### IV. DISCUSSION

Before we discuss the quadrupole splitting in more detail, we would first like to mention the changes in the electronic structure, concluded from isomer shift data,<sup>1</sup> because at first sight the two data might seem contradictory. From the isomer shift data we found an increasing number of  $s$  electrons at the  $^{57}\text{Fe}$  nucleus, when the Zr content increased. This means that an Fe atom is receiving more charge from an increasing number of Zr neighbors. It is just the electronic structure of this neighborhood, that is observed with the quadrupole splitting. The charge at a Zr atom is thinner than at an Fe atom. So the surrounding electron density, or the effective number of free electrons, which is more and more determined by the Zr atoms, decreases as a result of the thinner electron clouds at Zr atoms. Thus the information obtained from isomer shift and quadrupole splitting, is different with respect to the concentration dependence of the electronic structure. With the isomer shift we keep looking at the Fe atoms, whereas with the quadrupole splitting we observe a change from an Fe to a Zr surrounding.

We showed that the steep increase of the quadrupole splitting from 60 at. % Zr can be explained assuming that the effective number of free electrons first increases up to 55 at. % Zr and then decreases. Due to the growth of the molar volume with increasing Zr content the Lindhard screening length  $1/2k_f$  is nearly constant up to 55 at. % Zr (see Fig. 7, upper line). This results in the quadrupole splitting being nearly constant also. In the alloys with more than 55 at. % Zr the number of screening electrons diminishes and the screening length increases (Fig. 7). Consequently the quadrupole splitting increases with increasing Zr content.

The calculations have been done using an fcc-like nearest-neighbor cluster that is statistically disordered. In amorphous Tm-Tm alloys the structure is close packed and the coordination numbers are of the order of 12. So one may expect the fcc-like pseudocrystalline cluster (or the DRPHS cluster) the most realistic results. We could have used other pseudocrystalline clusters or a DRPHS

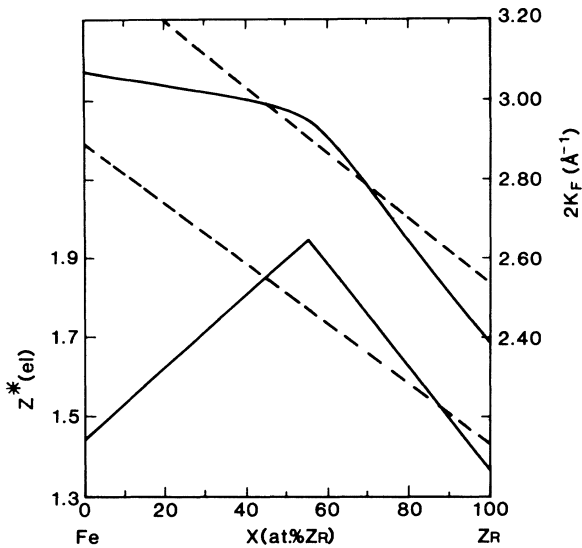


FIG. 7. Effective number of free electrons per atom  $Z^*$  (lower line) and  $2k_f$  (upper line) in amorphous  $\text{Fe}_{100-x}\text{Zr}_x$ ; the dashed lines indicate the region for  $2k_f$  in which a negative TCR can be expected.

cluster, but the results would have been essentially the same apart from the value of the antishielding enhancement factor  $\alpha$ .

A more serious limitation of the model is that in the derivation of the dielectric function we assume that we have a spherical Fermi surface. It is also assumed that this surface can be described with only one wave vector  $k_F$ . This certainly is not true since in amorphous alloys  $k$  is not a good quantum number, because of the lack of translation symmetry. One can amend these limitations by including in the dielectric function exchange and correlation terms and by evaluating it at a temperature different from 0 K; this will give a distribution of  $k_f$  values.

Finally, it is interesting to note that the total density of states demonstrates a similar behavior as the effective number of free electrons  $Z^*$ . Neddermeyer and Paul have measured the  $d$ -electron density of states using ultraviolet photoemission spectroscopy. They find that in  $\text{Fe}_{91}\text{Zr}_9$  this density of states is increasing up to the Fermi level, while in  $\text{Fe}_{33}\text{Zr}_{67}$  and  $\text{Fe}_{25}\text{Zr}_{75}$  it reaches a maximum somewhat below the Fermi level.<sup>21</sup> From this, one may conclude that the  $d$ -electron density of states at the

Fermi level first increases with Zr content and that it decreases with Zr content in Zr-rich alloys. Also the specific-heat measurements of Onn<sup>22</sup> and Matsuura<sup>23</sup> show that the  $d$ -electron density of states at the Fermi level decreases with increasing Zr content between at least 70 and 80 at. % Zr. If one accepts this correlation, one is led to an interpretation of  $Z^*$  as the number of electrons right at the Fermi surface. This interpretation differs from that of Eposito *et al.* who interpreted  $Z^*$  as the integrated free-electron component of the density of states at the Fermi level.<sup>9</sup>

## V. CONCLUSION

Finally, we conclude that we have shown that the concentration dependence of the quadrupole splitting in amorphous Fe-Zr alloys can be understood without assuming a structural transition. We only had to assume a transition in the electronic structure. Some evidence for this has been found in the literature from specific heat and ultraviolet photoemission spectroscopy experiments.

We have also seen that the sign and magnitude of the quadrupole splitting and asymmetry parameter in clusters with strong chemical order is affected by the conduction electron contribution to the EFG. The precise effect cannot be predicted in a simple way and depends strongly on the local order. We conclude that one cannot obtain structural information from the Mössbauer quadrupole splitting in amorphous metals, without additional information about the electronic structure. Therefore one has to be very careful to use the quadrupole splitting as a "fingerprint" of the structure, by comparing the values of amorphous alloys with those of crystalline alloys with a known structure.

## ACKNOWLEDGMENTS

The authors are very much indebted to Professor Dr. G. A. Sawatzky and Dr. I. Vincze for stimulating discussions, Professor Dr. K. H. J. Buschow is gratefully acknowledged for the longstanding cooperation and for providing the amorphous Fe-Zr samples. This work forms part of the research program of the Stichting voor Fundamenteel Onderzoek der Materie (Foundation for Fundamental Research on Matter FOM) and was made possible by financial support from the Nederlandse Organisatie voor Zuiver-Wetenschappelijk Onderzoek (Netherlands Organization for the Advancement of Pure Research, ZWO).

\*Present address: Philips Research Laboratories, NL-5600 MD Eindhoven, The Netherlands.

†Present address: Institut für Theoretische Physik, Technische Universität Wien, Karlplatz 13, A-1040 Wien, Austria.

<sup>1</sup>W. Hoving, P.M.L.O. Scholte, P. Dorenbos, G. A. Fokkema, E. A. G. Weits, F. van der Woude, I. Vincze, and K. H. J. Buschow, *Phys. Rev. B* **32**, 8368 (1985).

<sup>2</sup>I. Vincze, F. van der Woude, and M. G. Scott, *Solid State*

*Commun.* **37**, 567 (1981); H. G. Wagner, M. Ghafari, H.-P. Klein, and U. Gonser, *J. Non-Cryst. Solids* **61/62**, 427 (1984); C. Michaelsen, H. A. Wagner, and H. C. Freyhardt, *J. Phys. F* **16**, 109 (1986); F. Aubertin, U. Gonser, S. J. Campbell, and H.-G. Wagner, *Z. Metallkd.* **76**, 237 (1985); G. Le Caer, J. M. Cadogan, R. A. Brandt, J. M. Dubois, and H. J. Güntherodt, *J. Phys. F* **14**, L73 (1984); M. Maurer and J. M. Friedt, and J. P. Sanchez, *J. Phys. F* **15**, 1449 (1985); M. Maurer and J. M.

- Friedt, *Hyperfine Interact.* **27**, 135 (1986).
- <sup>3</sup>T. P. Das and M. Pomerantz, *Phys. Rev.* **123**, 2070 (1961).
- <sup>4</sup>R. S. Raghavan, E. N. Kaufman, and P. Raghavan, *Phys. Rev. Lett.* **34**, 1280 (1975).
- <sup>5</sup>R. Vianden, *Hyperfine Interact.* **15/16**, 189 (1983).
- <sup>6</sup>H. C. Verma, J. Chappert, and G. N. Rao, *Hyperfine Interact.* **11**, 45 (1981).
- <sup>7</sup>E. N. Kaufmann and R. Vianden, *Rev. Mod. Phys.* **51**, 161 (1979).
- <sup>8</sup>W. Witthuhn and W. Engel, in *Hyperfine Interactions of Radioactive Nuclei*, edited by J. Christiansen (Springer-Verlag, Berlin, 1983), p. 205.
- <sup>9</sup>E. Eposito, H. Ehrenreich, and G. D. Gelatt, *Phys. Rev. B* **18**, 3913 (1978).
- <sup>10</sup>C. A. Sholl, *Proc. Phys. Soc. London* **91**, 130 (1967).
- <sup>11</sup>J. L. Finney, *Proc. R. Soc. London, Ser. A* **319**, 479 (1970); C. H. Bennett, *J. Appl. Phys.* **43**, 2727 (1972).
- <sup>12</sup>G. S. Cargill III, in *Solid State Physics*, edited by H. Ehrenreich, F. Seitz, and D. Turnbull (Academic, New York, 1975), Vol. 30, p. 227.
- <sup>13</sup>Gy. Faigel, W. H. de Vries, H. J. F. Jansen, M. Tegze, and I. Vincze, in *Proceedings of the Conference on Metallic Glasses: Science and Technology*, Budapest, 1980, edited by C. Hargitai, I. Bakonyi, and T. Kemeny (unpublished), p. 275.
- <sup>14</sup>A. R. Miedema and A. K. Niessen, *Physica B+C* **114B**, 367 (1982).
- <sup>15</sup>P. M. L. O. Scholte, Ph.D. thesis, University of Groningen, 1987.
- <sup>16</sup>M. Tegze, R. A. de Groot, F. van der Woude, and F. M. Mueller, in *Proceedings of the Fifth International Conference on Rapidly Quenched Metals*, edited by S. Steeb and H. Warlimont (Elsevier, Amsterdam, 1985), p. 1031.
- <sup>17</sup>A. M. van der Kraan and K. H. J. Buschow, *Phys. Rev. B* **27**, 2693 (1983).
- <sup>18</sup>I. Vincze, *Nucl. Instrum. Meth.* **199**, 247 (1982).
- <sup>19</sup>K. H. J. Buschow and P. H. Smit, *J. Magn. Magn. Mater.* **23**, 85 (1981); K. H. J. Buschow and N. M. Beekmans, *Phys. Rev. B* **19**, 3843 (1979).
- <sup>20</sup>K. Nishiyama and D. Riegel, *Phys. Lett. A* **57**, 270 (1976).
- <sup>21</sup>H. Neddermeyer and Th. Paul, *Phys. Rev. B* **36**, 4148 (1987).
- <sup>22</sup>D. G. Onn, L. Q. Wang, and K. Fukamichi, *Solid State Commun.* **47**, 479 (1983).
- <sup>23</sup>M. Matsuura, U. Mizutani, and K. Fukamichi, in *Proceedings of the Fifth International Conference on Rapidly Quenched Metals*, edited by S. Steeb and H. Warlimont (Elsevier, Amsterdam, 1985), p. 1019.